Converging shock wave focusing and interaction with a target

M. Nitishinskiy,[1] S. Efimov,[1] O. Antonov,[1] D. Yanuka,[1] V. Tz. Gurovich,[1] V. Bernshtam,[2] V. Fisher,[2] and Ya. E. Krasik[1]
[1]*Physics Department, Technion, Haifa 32000, Israel*
[2]*Weizmann Institute of Science, Rehovot 76100, Israel*

(Received 11 February 2016; accepted 31 March 2016; published online 18 April 2016)

Converging shock waves in liquids can be used efficiently in the research of the extreme state of matter and in various applications. In this paper, the recent results related to the interaction of a shock wave with plasma preliminarily formed in the vicinity of the shock wave convergence are presented. The shock wave is produced by the underwater electrical explosion of a spherical wire array. The plasma is generated prior to the shock wave's arrival by a low-pressure gas discharge inside a quartz capillary placed at the equatorial plane of the array. Analysis of the Stark broadening of H_α and H_β spectral lines and line-to-continuum ratio, combined with the ratio of the relative intensities of carbon C III/C II and silicon Si III/Si II lines, were used to determine the plasma density and temperature evolution. It was found that during the first ~200 ns with respect to the beginning of the plasma compression by the shock wave and when the spectral lines are resolved, the plasma density increases from $2 \times 10^{17}\,cm^{-3}$ to $5 \times 10^{17}\,cm^{-3}$, while the temperature remains at the same value of 3–4 eV. Further, following the model of an adiabatically imploding capillary, the plasma density increases $>10^{19}\,cm^{-3}$, leading to the continuum spectra obtained experimentally, and the plasma temperature >30 eV at radii of compression of $\leq 20\,\mu m$. The data obtained indicate that the shock wave generated by the underwater electrical explosion of a spherical wire array retains its uniformity during the main part of its convergence. *Published by AIP Publishing.*
[http://dx.doi.org/10.1063/1.4946864]

I. INTRODUCTION

Convergence of cylindrical or spherical shock waves (SWs)[1] allows one to achieve extreme states of matter in the vicinity of implosion axis or origin. Therefore, the subject of converging SWs continues to be a significant topic of experimental and theoretical research. The vital question remains the SW front uniformity which determines the maximal achievable parameters of the matter compressed by this SW. In addition, spherical converging SWs are considered to drive magnetized target fusion,[2] and as such SWs have several industrial and medical applications.[3,4] Converging SWs can be generated by laser pulses,[5] piston impacts,[2] reflection of divergent waves,[6] or underwater explosion of spherical foils or wire arrays.[7] The latter approach is rather attractive because it provides a relatively good (~24%) efficiency of energy transfer to the water flow by the exploded and expanding wires.

The recent results of research on the underwater electrical explosion of single wire and wire arrays were presented in the reviews.[8,9] It was found that sub-μs and μs-timescale electrical explosions of spherical wire arrays result in the generation of converging SW. Numerical simulations regarding the SW front's stability showed that it retains its symmetry with respect to the corrugated linear perturbations because of the low compressibility of water.[10] The results of experiments and hydrodynamic numerical simulations, coupled with the equation of state (EOS) for wire material and water, indicate[11] that the convergence of the SW results in an extreme state of water in the vicinity of the SW implosion. Namely, using pulse generators with a stored energy of only ~5 kJ, one can expect a pressure, temperature, and density of water of 2×10^{12} Pa, ~10 eV, and 8 g/cm^3, respectively, at a radius of convergence $\leq 6\,\mu m$. Thus, using modern powerful pulsed generators with stored energy of hundreds of kJ, one can expect to obtain values of pressure $>2 \times 10^{12}$ Pa and temperatures >100 eV in significantly larger volumes of compressed water.[8] However, the main problem not resolved yet is the uniformity of the converging SW front, especially in the vicinity of convergence when the shock wave becomes radiative.

In order to confirm the uniform convergence of the SW, optical emission spectroscopy was applied to study the parameters of the plasma in the vicinity of the SW implosion.[12] In these experiments, a Cu capillary was placed at the equatorial plane of the spherical wire array. The SW approaching the inner surface of the capillary wall leads to intense evaporation of Cu atoms. This Cu atom flow fills the entire volume of the capillary within $\leq 10^{-7}$ s and is compressed adiabatically by the implosion of the capillary that acquires velocity behind the SW front. Analysis of the spectral lines shapes and intensities allows one to estimate the average Cu plasma temperature and density as 0.68 ± 0.2 eV and $(3 \pm 1) \times 10^{16}\,cm^{-3}$, respectively. Thus, this research showed that the SW generated by spherical wire array explosion experiences convergence leading to increased energy density deposition in the vicinity of the SW's implosion.

In this paper, we present the results of the evolution of the parameters of the plasma under interaction with converging SW generated by the same underwater electrical spherical wire array explosion as that described in Ref. 12. However, opposite to earlier research,[12] in the present experiment the plasma in the vicinity of the SW's implosion origin is generated before the SW's convergence. Studying

plasma parameters before the SW's convergence, this approach allows one to obtain the evolution of the plasma parameters during the SW's implosion resulting in a better understanding of the SW's convergence uniformity. In addition, this method allows one to control the plasma parameters before the SW's convergence using different types of gas, discharge current amplitude, and time delay between the beginning of the plasma and the SW generation.

In the present experiment, the plasma was generated by a low-pressure gas (C_3H_8) discharge in a quartz capillary placed in the equatorial plane of the array prior to the SW interaction with the capillary, thus allowing the plasma parameters prior to and during SW interaction to be studied. As in previous experiments,[12] the intense evaporation of the capillary inner wall material allowed the oxygen and silicon spectral lines to be observed. The Stark broadenings of the H_α and H_β lines were used to determine the plasma density, and NOMAD[13] collisional-radiative (CR) modeling was used to extract the electron temperature of the equilibrium plasma, which has the same ratio of the intensities of different carbon spectral lines as obtained in the experiment. In addition, the intensities of the silicon spectral lines were applied to estimate the plasma electron temperature.

II. EXPERIMENTAL SETUP AND DIAGNOSTICS

The experimental setup is shown in Fig. 1. The 30-mm diameter spherical wire array that was used consisted of 40 Cu wires, each 100 μm in diameter. The array was installed in a stainless steel chamber filled with de-ionized water and having windows for optical access. To explode the arrays, a high-current pulse generator[14] was used. The generator was charged up to 27 kV (stored energy of ~3.6 kJ), resulting in a discharge current amplitude of ~300 kA and rise time of ~1.1 μs measured by a self-integrated Rogowski coil at short-circuit load having ~15 nH inductance.

A quartz capillary with outer and inner diameters of 3 mm and 2 mm, respectively, was placed at the equatorial plane of the spherical array. Two electrodes (a stainless steel anode and a Cu capillary cathode) were inserted into the quartz capillary. A ~1.5 mm gap between the electrodes was located symmetrically to the sphere origin. The capillary was evacuated to a pressure of ~0.2 Pa and then filled with a C_3H_8 gas flow up to a pressure of ~40 Pa. The spark gas discharge was driven using a pulse generator producing at its output a pulse with a current and voltage amplitude of 320 A and 13 kV, respectively, and a rise time of ~3.5 μs.

The parameters of the plasma were measured using a 1-mm diameter optical fiber inserted through the copper electrode to collect the light from the discharge gap. The fiber was located at a distance of 0.5 mm from the open edge of the Cu electrode (see Fig. 1). The plasma light emission was guided by the fiber outside the experimental chamber and directed to the inputs of two spectrometers and a photomultiplier tube (PMT), using a beam splitter, mirrors, and lenses. A 0.5 m focal length Chromex-500 (2400 grooves/mm or 1800 grooves/mm) and a 0.25 m focal length Chromex-250 (1800 grooves/mm or 1200 grooves/mm grating) imaging spectrometer and a Hamamatsu R6095 PMT with 6560 Å ± 50 Å filter were used in this study. The images of the spectral lines at the output of both spectrometers were obtained using two intensified 4QuikE cameras (Stanford Computer Optics) operating with a frame duration of 500 ns. To calibrate the spectroscopic setup, Oriel spectral lamps were used. The beginning of the spark gas discharge was set to be ~2.0 μs prior to the camera frame. The spectra were registered for only the spark discharge ("prior to shot") and then for the plasma compressed by the SW ("in shot").

Synchro-pulses from the 4QuikE cameras, PMT, spark discharge, and the main pulse generator currents were acquired by two Tektronix TDS-2024 digitizing oscilloscopes. Typical waveforms of the array and gas discharge currents, synchro-pulse, and PMT signals are shown in Fig. 2. One can see that the amplitude of the array discharge current prior to the wire explosion reaches ~220 kA during ~0.9 μs. The spark gas gap discharge starts at ~5.5 μs with respect to the beginning of the array current and the spark current amplitude reaches ~320 A (current density of ~10 kA/cm^2). In addition, one can see a rather slow gradual

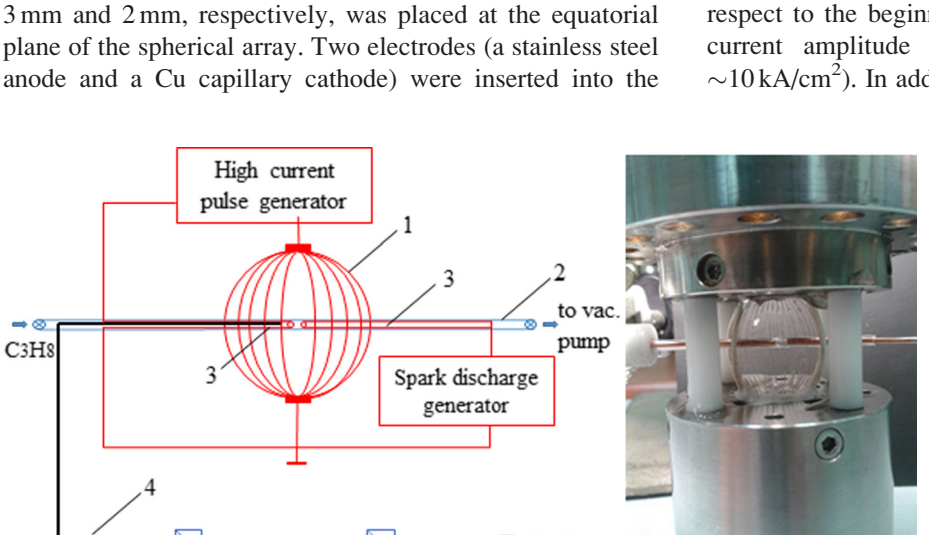

FIG. 1. Experimental setup: 1—spherical wire array, 2—capillary, 3—electrodes, 4—fiber output. Right: photo of the wire array with inserted capillary.

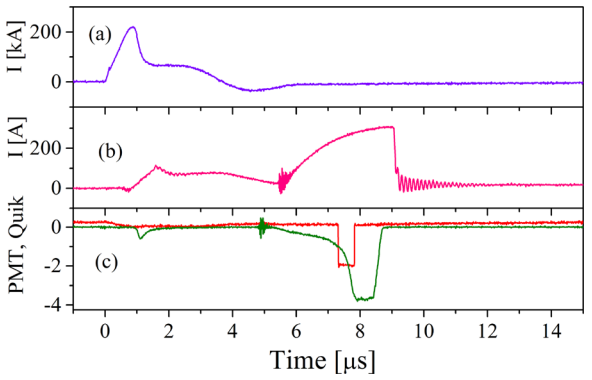

FIG. 2. Typical waveforms of the array (a) and gas discharge currents (b), and synchro-pulse (red) and PMT (green) signals (c).

increase in light emission intensity registered by the PMT due to the increase in the discharge current, with a drastic increase in light intensity at time ($\sim$7.4 μs) when the SW approaches the quartz tube. Finally, at $\sim$8.4 μs this light emission decreases corresponding to the termination of the discharge current at $\sim$9 μs caused by the complete destruction of the quartz capillary by the SW.

III. EXPERIMENTAL RESULTS

In earlier experiments,[12] it was shown that the light emission from the capillary appears when the SW approaches the origin of its implosion. In the present research, the obtained spectra were divided into three groups according to the time delay between the frame termination and the maximum in the light emission registered by the PMT. The synchro-pulses of the 4QuikE cameras with different time delays shown in Fig. 3 correspond to these three types of spectra.

(1) At time delays >500 ns, the spectra obtained "in shot" were almost the same as those obtained "prior to shot." These data coincide with the results of 1D hydrodynamic simulations[9,12] of the SW convergence, showing that in the case of an SW uniform spherical implosion, at a time delay of $\sim$500 ns, the SW just approaches the capillary.

(2) At time delays in the range 300 ns–500 ns, the spectral lines obtained "in shot" experienced significant broadening and increased in intensity as compared with the same spectral lines obtained "prior to shot." In addition, strong intensity spectral lines O II, Si II, and Si III appeared, which were very weak in the "prior to shot" spectra. Examples of the spectra "prior to shot" and "in shot" are shown in Fig. 4. These data strongly indicate an increase in plasma density and the evaporation of oxygen and silicon atoms from the inner surface of the quartz capillary as a result of the SW's impact with the capillary.

(3) At time delays <300 ns, the spectral lines become almost not resolved and only an intense continuum spectrum was obtained (see Fig. 8). Thus, one can suggest that at these time delays, plasma density and temperature increase significantly as a result of the compression by the imploding capillary, resulting in the disappearance of the spectral lines in the visible range of light.

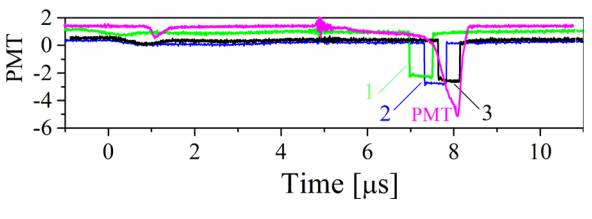

FIG. 3. Example of three frames of 4QuikE camera at different time delays with respect to the maximum of the light intensity registered by the PMT.

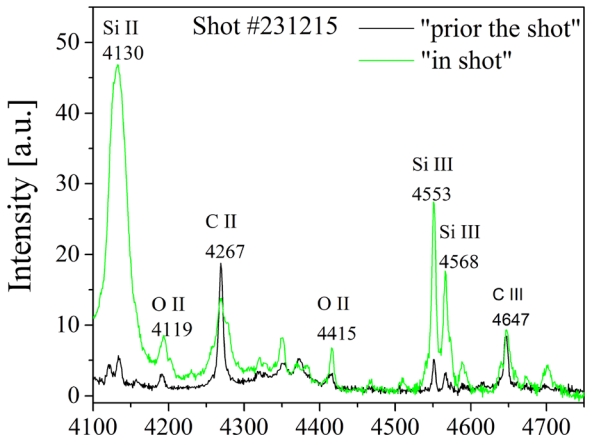

FIG. 4. Examples of "in shot" spectrum obtained at time delays in the range 300 ns–500 ns (green) and "prior to shot" spectrum (black). Wavelength in Å.

In the experiments on plasma density estimation using Stark broadening, Chromex-500 and Chromex-250 spectrometers (both with 1800 groove/mm gratings) were used for H_α and H_β spectral line observations, respectively. In order to obtain C II 4267 Å and C III 4647 Å spectral lines simultaneously in one shot, the 4100–4750 Å spectral range of the Chromex-250 spectrometer was used. The ratio of the intensities of these spectral lines was used to determine the plasma electron temperature assuming the local thermodynamic equilibrium (LTE) model. In addition, the continuum spectrum obtained at a time delay <300 ns was used to estimate the plasma density. Here let us note that since all spectra are time-integrated over several hundreds of nanoseconds, the obtained values of temperature and density of plasma can be considered only as "mean" values.

A. Electron density measurements

Typical profiles of H_α spectral line light intensity obtained "prior to shot" and "in shot" at a time delay of 300 ns are shown in Fig. 5.

A Voigt function was used to fit the H_α line profile. The Stark broadening contribution is described by the Lorentzian component of the Voigt function, whereas the Doppler and instrumental broadenings are described by the Gaussian component. The Doppler broadening for the H_α line assuming temperatures <5 eV does not exceed 1.2 Å and instrumental broadening has a Full Width at Half Maximum (FWHM) of $\sim$1.3 Å. Thus, one can calculate the Lorentzian FWHM "prior to shot" as 19 ± 2 Å and "in shot" as 31 ± 4 Å. Using tabulated data[15] for H_α spectral line broadening versus the plasma electron density, which has a rather

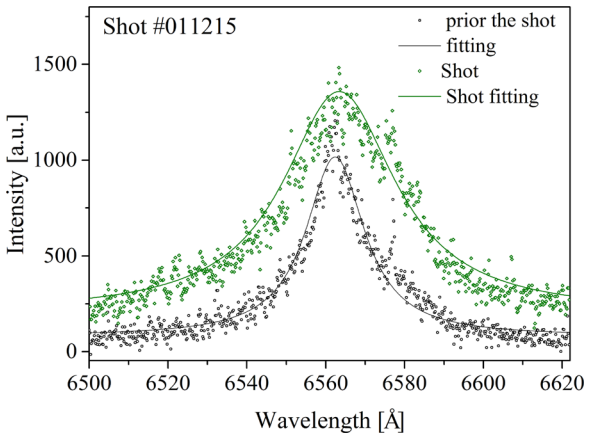

FIG. 5. Typical profiles of H_α spectral line light intensity obtained "prior to shot" and "in shot" at the time delay of 300 ns.

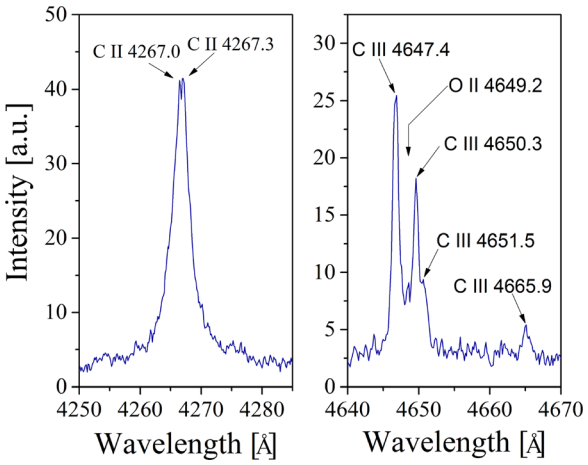

FIG. 6. Typical spectral lines of C II and C III ions prior the shot. 0.5 m focal length spectrometer with 2400 grooves/mm grating.

weak dependence on temperature in the range 2–5 eV, the density of the plasma was estimated as $(2.1 \pm 0.5) \times 10^{17}\,\mathrm{cm}^{-3}$ and $(4.5 \pm 1.0) \times 10^{17}\,\mathrm{cm}^{-3}$ "prior to shot" and "in shot," respectively. In addition, one can see in Fig. 5 red shifts of the center of the H_α line. These shifts can be estimated as 0.8 ± 0.6 Å "prior to shot" and ~1.5 Å "in shot." According to the data presented in Ref. 16, these red shifts correspond to approximately the same range of electron density as was obtained using Stark broadening of the H_α line. Similar results for plasma density "prior to shot" and "in shot" were obtained using the analysis of the Stark broadening of the H_β spectral lines. However, the accuracy of this analysis was significantly less than in the case of H_α because of the smaller intensity of the H_β spectral line as compared with the intensity of the continuum spectrum.

B. Plasma electron temperature

The plasma electron temperature was determined using the relative intensities of the C II (4267 Å) and C III (4647 Å) carbon ions spectral lines (see Fig. 4) obtained by a Chromex-250 spectrometer with a 1200 grooves/mm grating. In this analysis, the spectral sensitivity of the spectrometer and of the photocathode of the 4QuikE framing camera also was used. The ratio of the C III/C II line intensities in the "prior to shot" and "in shot" experiments was found to be 0.3 ± 0.1 and 0.5 ± 0.1, respectively. Typical spectral intensity profiles of the C II and C III lines are shown in Fig. 6. One can see that the C II spectral line is in fact composed of several degenerate transitions and that the C III spectral line profile is partially overlapped by the O II spectral line.

Following Griem,[17] one can estimate that a plasma electron density $>2 \times 10^{17}\,\mathrm{cm}^{-3}$ is sufficient for local thermodynamic equilibrium (LTE) and the time required for achieving this LTE does not exceed a few tens of nanoseconds. Thus, considering LTE, the electron temperature can be obtained using the ratio of C III/C II line intensities[17]

$$\frac{I_{CII}}{I_{CIII}} = \frac{4}{n_e}\left(\frac{mkT}{2\pi\hbar}\right)^{3/2} \frac{A_{CII} g_{CII} \lambda_{4647}}{A_{CIII} g_{CIII} \lambda_{4267}} \times \exp\left(\frac{E_{CIII} + E_\infty - E_{CII} - \Delta E_\infty}{kT}\right),$$

where I is the measured integrated line intensity, A is the Einstein coefficient for spontaneous emission, λ is the transition wavelength, g is the statistical weight of the upper energy level, E_{CIII} is the upper energy level of the C III ion excited state, E_{CII} is the upper energy level of the C II ion excited state, E_∞ is the ionization energy of C II ion, and ΔE_∞ is a correction factor for the ionization energy. n_e and T are the plasma electron density and temperature, respectively, and k and $\hbar$ are the Boltzmann's and Planck's constants, respectively.

In order to account for the different possible transitions from excited energy states, the collisional-radiative (CR) code NOMAD[13] was also used. In this case, the parameters of the equilibrium plasma, which has the same ratio of the intensities of the lines as obtained in the experiment, were determined for the plasma electron density obtained from the Stark broadening of Balmer lines. An example of the results of these simulations is shown in Fig. 7.

These two methods gave almost the same plasma electron temperature. Namely, the plasma electron temperature "prior to shot" and "in shot" was found to be (3.8 ± 0.5) eV and (4.2 ± 0.5) eV, respectively. In addition, two silicon lines Si II (4128 Å) and Si III (4553 Å) were used to estimate the plasma electron temperature based on LTE approximation. The latter also results in a ~3 eV electron temperature for both the "prior to shot" and "in shot" case. Thus, one can see that the SW interaction with the preliminary generated plasma does not lead to significant increasing of electron temperature.

C. Plasma parameter determination by continuum spectrum

A bright continuum spectrum appears at time delays <300 ns, although a weak continuous background was already present in spectra obtained at time delays >300 ns. The appearance of this bright continuum spectrum can be associated with intense evaporation of the capillary material and its simultaneous compression by the adiabatic implosion of the quartz capillary. The latter leads to an increase in the

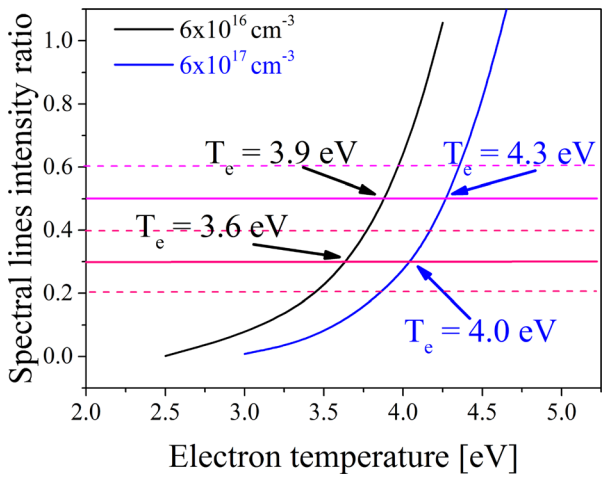

FIG. 7. Ratio of the lines intensity (C III 4647 Å/C II 4267 Å) versus the plasma electron temperature for two values of the plasma electron density (steady state calculation).

density and temperature of the plasma, in particular, at the final stage of the implosion.

Indeed, at time delays <300 ns only traces of the H_α line were observed (see Fig. 8), while H_β either merged with continuum spectrum due to the Stark broadening or disappeared due to the lowering of ionization threshold below its upper level. For observed signal-to-noise ratio and $T_e \approx T_i \approx 3$ eV, the disappearance of Stark-broadened H_β points to $n_e > 4 \times 10^{18}\,\mathrm{cm}^{-3}$. In the computations of Stark width, we followed Ref. 18. Using Stark widths and Inglis-Teller approach[19,20] to the computation of density-dependent ionization threshold, we found that the threshold cuts upper level of H_β at $n_e \sim 5 \times 10^{18}\,\mathrm{cm}^{-3}$, thus both mechanisms point to $n_e > 4 \times 10^{18}\,\mathrm{cm}^{-3}$.

We analyzed the effect of density on the evolution and disappearance of spectral lines using collisional-radiative computations for plasma of H, C, and Si mixture. For example, Fig. 8 displays H_α emitted from plasma sphere with $T_e \approx T_i \approx 3$ eV in collisional-radiative equilibrium (CRE). In particular, the simulations showed that H_α merges with

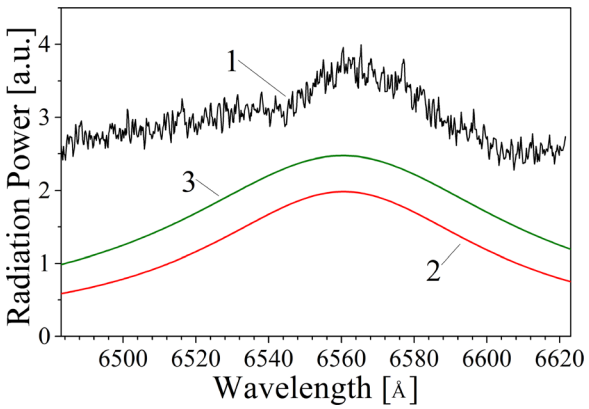

FIG. 8. Experimentally measured and simulated spectrum of the plasma for different densities. 1—Experimental line shape. 2—Simulation of the power from plasma: hydrogen ($1.2 \times 10^{18}\,\mathrm{cm}^{-3}$) + carbon ($4 \times 10^{17}\,\mathrm{cm}^{-3}$) + silicon ($10^{16}\,\mathrm{cm}^{-3}$). $Z_H = 0.986$, $Z_C = 1.773$, $Z_{Si} = 2.401$; $n_e = 1.9 \times 10^{18}\,\mathrm{cm}^{-3}$. Spherical plasma of radius R = 1 mm. $T_e = T_i = 3$ eV. 3—The same simulation with higher silicon density ($4 \times 10^{17}\,\mathrm{cm}^{-3}$). $Z_H = 0.980$, $Z_C = 1.700$, $Z_{Si} = 2.305$; $n_e = 2.78 \times 10^{18}\,\mathrm{cm}^{-3}$.

continuum at $n_e \sim 10^{19}\,\mathrm{cm}^{-3}$. Based on detailed comparisons of experimental data to simulated spectra, we concluded that the electron density at this stage of implosion is about $5 \times 10^{18}\,\mathrm{cm}^{-3}$.

IV. DISCUSSION

The results of the present research show that the interaction of converging SW with preliminary formed plasma leads to a ~2.3-fold increase in its density, while keeping almost the same temperature. The latter can be explained by the intense evaporation of mainly neutral atoms of oxygen and silicon from the internal wall of the quartz capillary when the SW is approaching that location. This cold flow of neutrals could keep plasma temperature almost unchangeable in spite of its heating by the converging SW. In addition, it was shown that later in time the plasma density and possible temperature increase significantly, which can be explained by the adiabatic implosion of the quartz capillary.

Let us apply the model of adiabatic implosion of the capillary, described in detail in Ref. 12. This model considers a converging SW propagating in water toward the capillary, which in the present experiments is quartz, with outer and inner radii $R = 1.5$ mm and $R = 1.0$ mm, respectively. The result of 1D hydrodynamic simulations of the SW convergence showed that the pressure at the water-quartz boundary at $R = 1.5$ mm reaches $P_w \sim 8.3 \times 10^9$ Pa because of the partial reflection of the SW from the capillary. The same pressure $P_c \sim 8.3 \times 10^9$ Pa is obtained behind the SW front penetrating the capillary wall. This allows one to estimate the quartz compression at that location $\delta_c = \rho_c/\rho_{0c} \approx 1.29$, where $\rho_{0c} \approx 2.2 \times 10^3\,\mathrm{kg/m}^3$ is the normal quartz density, $\rho_c = 2.83 \times 10^3\,\mathrm{kg/m}^3$ is the density of compressed quartz, using the equation of state for quartz (Ref. 21): $P_c \approx B(\delta_c^{2.6} - 1)$, where the constant $B \approx 9 \times 10^9$Pa. The plane SW propagation velocity in quartz can be found as $Dc = V_0\sqrt{(P - P_0/(V_0 - V)} \approx 4.12 \times 10^3$ m/s, where $V_0 = 1/\rho_0$ and $V = 1/\rho$ are the unit volumes of normal and compressed quartz, respectively. However, in the case of cylindrical geometry the value of the SW velocity depends on the radius. Using the self-similarity approach,[22] the time-dependent radius of the SW front can be presented as $R(t) \approx C(t_0 - t)^\alpha$, $R(t=0) = 1.5$ mm with the self-similarity parameter $\alpha \approx 0.78$, for a cylindrical wave in quartz and $t_0 \approx R(t=0)/\alpha D_c$ is the time which the SW requires to propagate in quartz to reach $R = 0$. Thus, the SW velocity can be defined as $D_c = dR/dt = -\alpha C(t_0 - t)^{\alpha-1}$. Using $D_c\ (t=0) = 4.12 \times 10^3$ m/s, one obtains that the SW front reaches the inner capillary boundary in ~200 ns with a front velocity $D_c^1 \approx 4.62 \times 10^3$m/s. Propagation of the SW inside the quartz leads to the flow of the material behind the SW front. At the inner boundary of the capillary, the compression and pressure of the quartz reach $\delta_c \approx 1.45$ and $P_c(R = 1) \approx 1.46 \times 10^{10}$ Pa.

The pressure of the plasma inside the capillary is significantly smaller than that at its inner radius. Therefore, one can consider that re-loading of the SW as it approaches the inner radius of the capillary leads to almost a doubling of the velocity of the quartz material toward the axis, $U_g \approx 2.92 \times 10^3$ m/s,

due to transfer of the energy of the SW to the kinetic energy of the quartz material at that location. The implosion of the capillary generates the SW propagating through the plasma inside the capillary. This process leads to additional plasma heating. However, estimations similar to those described in Ref. 12 showed that the plasma temperature increases to only ~0.5 eV. This result agrees satisfactorily with the experimentally obtained insignificant increase in the plasma temperature during the SW interaction with the plasma.

The problem of the implosion of the capillary is similar to the problem of cavity collapse (see e.g., Ref. 23). Following the self-similarity analysis, the capillary boundary radius decreases as $R(t) = C_1(t_c - t)^{0.78}$, with the pressure equal zero at the time-dependent inner radius of the capillary. Here, the notation t_c corresponds to time of collapse, i.e., the time when the inner boundary of the capillary reaches the axis of implosion; t is the time measured from the moment when the SW propagating in the quartz reaches the inner capillary boundary. Applying the same method as was used to estimate the time that SW requires to reach the inner boundary of the capillary, one obtains $t_c \approx 0.78R(1\,\text{mm})/U_g \approx 270\,\text{ns}$.

The implosion of the capillary leads to the adiabatic compression and heating of the plasma inside the capillary. Simulations showed that at the time when the SW, generated in the plasma by the imploding capillary, reaches its axis, the inner radius of the capillary approaches $R = 0.3\,\text{mm}$. Using the adiabatic compression approach, one can now estimate the pressure, temperature, and density of the plasma during the capillary implosion. In the case of adiabatic compression of monatomic gas (adiabatic index $\gamma = 1.7$), the increase in the gas temperature and pressure versus the imploding radius can be estimated as $T_2 = T_1(R_1/R_2)^{2(\gamma-1)}$ and $P_2 = P_1(R_1/R_2)^{2\gamma}$, resulting in $T_2 = 38\,\text{eV}$ and $P_2 = 5.1 \times 10^8\,\text{Pa}$ at $R_2 = 0.02\,\text{mm}$ for $R_1 = 0.3\,\text{mm}$ and $T_1 = 2.5\,\text{eV}$ and $P_1(R_1 = 0.3\,\text{mm}) = 5.5 \times 10^4\,\text{Pa}$. The density of the particles also increases significantly, reaching $\sim 3 \times 10^{17}\,\text{cm}^{-3}$. In the case of a temperature of ~30 eV, one can expect a plasma electron density of $\sim 10^{18}\,\text{cm}^{-3}$. This drastic increase in the pressure, density, and temperature of the plasma leads to the continuous spectra obtained in the experiments. Let us note here that these estimates show only the low boundary of the values of the plasma density because atoms evaporated from the quartz were not taken into account.

V. SUMMARY

Carried out experimental research showed that the heating and compression of the preliminary generated plasma can be achieved by the converging SW formed by an underwater electrical explosion of a spherical wire array. By using an analysis of the spectral lines obtained and the continuum spectrum, the density and temperature of the plasma were determined at different stages of the plasma compression. It was also shown that the SW penetration of the inner wall of the capillary leads to intense evaporation of the wall material and its adiabatic compression by the imploding capillary. The time of the SW implosion and the energy deposition into the plasma thus obtained are in good agreement with the results of the theoretical model, thus indicating on uniformity of the converging SW front. Due to its high sensitivity, this approach of measurement of incident SW parameters can be used in experiments when significantly more powerful pulsed generators will be applied.

ACKNOWLEDGMENTS

The authors are grateful to A. Meller for technical support. This research was supported by the Israeli Science Foundation Grant No. 99/12.

[1]M. Van Dyke and A. J. Guttmann, J. Fluid Mech. **120**, 451 (1982).
[2]M. Laberge, J. Fusion Energy **27**, 65 (2008).
[3]K. Takayama and T. Saito, Annu. Rev. Fluid Mech. **36**, 347 (2004).
[4]S. H. R. Hosseini, S. Iwasaki, T. Sakugawa, and H. Akiyama, J. Korean Phys. Soc. **59**, 3526 (2011).
[5]T. Pezeril, G. Saini, D. Veysset, S. Kooi, P. Fidkowski, R. Radovitzky, and K. A. Nelson, Phys. Rev. Lett. **106**, 214503 (2011).
[6]M. Müller, Acustica **64**, 85 (1987).
[7]O. Antonov, L. Gilburd, S. Efimov, G. Bazalitzky, V. Tz. Gurovich, and Ya. E. Krasik, Phys. Plasmas **19**, 102702 (2012).
[8]Ya. E. Krasik, A. Grinenko, A. Sayapin, S. Efimov, A. Fedotov, V. Tz. Gurovich, and V. Oreshkin, IEEE Trans. Plasma Sci. **36**, 423 (2008) and references therein.
[9]Ya. E. Krasik, S. Efimov, D. Sheftman, A. Fedotov-Gefen, O. Antonov, D. Shafer, D. Yanuka, M. Nitishinskiy, M. Kozlov, L. Gilburd, G. Toker, S. Gleizer, E. Zvulun, V. Tz. Gurovich, D. Varentsov, and M. Rodionova, IEEE Trans. Plasma Sci. **44**(4), 412 (2016).
[10]M. Kozlov, V. Tz. Gurovich, and Ya. E. Krasik, Phys. Plasmas **20**, 112701 (2013).
[11]O. Antonov, S. Efimov, D. Yanuka, M. Kozlov, V. Tz. Gurovich, and Ya. E. Krasik, Appl. Phys. Lett. **102**, 124104 (2013).
[12]O. Antonov, S. Efimov, V. Tz. Gurovich, and Ya. E. Krasik, Phys. Plasmas **22**, 053507 (2015).
[13]Yu. V. Ralchenko and Y. Maron, J. Quant. Spectrosc. Radiat. Transfer **71**, 609 (2001).
[14]S. Efimov, A. Fedotov, S. Gleizer, V. Tz. Gurovich, G. Bazalitski, and Ya. E. Krasik, Phys. Plasmas **15**, 112703 (2008).
[15]M. Gigosos and V. Cardenoso, J. Phys. B: At. Mol. Opt. Phys. **29**, 4795 (1996).
[16]C. Parigger and E. Oks, Int. Rev. At. Mol. Phys. **1**, 13 (2010).
[17]H. R. Griem, *Spectral Line Broadening by Plasmas* (Academic Press, New York, 1974).
[18]E. Stambulchik and Y. Maron, Phys. Rev. E **87**, 053108 (2013).
[19]D. R. Inglis and E. Teller, Astrophys. J. **90**, 439 (1939).
[20]H. R. Griem, *Principles of Plasma Spectroscopy* (Cambridge, 1997).
[21]F. A. Baum, L. P. Orlenko, K. P. Stanyukovich, V. P. Chelyshev, and B. I. Shekhter, *Physics of Explosion* (Nauka, Moscow, 1975).
[22]V. Ts. Gurovich and L. G. Fel, JETP Lett. **89**, 14 (2009).
[23]C. Hunter, J. Fluid Mech. **8**, 241 (1960).